Absolute flow field estimation for the Nordic seas from combined gravimetric, altimetric, and in situ data

Absolute flow field estimation for the Nordic seas from combined gravimetric, altimetric, and in situ data

A. Hunegnaw,[1] F. Siegismund,[2,3] R. Hipkin,[1] and K. A. Mork[4,5]

Received 29 February 2008; revised 27 November 2008; accepted 17 December 2008; published 27 February 2009.

[1] In the Nordic seas, we combine a computation of absolute surface current flow derived from geodetic data with in situ historical hydrographic data to estimate the absolute volume, heat, and salt transports as a function of depth. Our mean dynamic topography (MDT) is calculated from marine, airborne and satellite gravimetry, combined with satellite altimetry, using a new algorithm called the iterative combination method (ICM). Residual noise in the gravimetric geoid is the limit on MDT resolution and is suppressed using a Gaussian filter with a width at half-peak amplitude of 59 km. Detailed and coherent flow paths for surface geostrophic currents are clearly identified. ICM MDT was used as fixed boundary condition to transform historical hydrography into absolute estimates of volume, heat, and salt transport, replacing the assumption of an isobaric surface at a predetermined depth. For the inflow of Atlantic Water (potential temperature $\Theta > 6°C$) through the Faroe-Shetland Channel into the Nordic seas, we obtain time-averaged fluxes between 1993 and 1996 of 3.5 Sv (volume), 121 TW (heat), and 124×10^6 kg s^{-1} (salt), very close to reported observations from acoustic Doppler current profiler moorings and conductivity-temperature-depth data. For the Svinøy section, we obtain a northward transport of Atlantic Water ($S > 35.0$, $T > 5.0°C$) of 3.9 Sv in the eastern branch of the Norwegian Atlantic Current comparable with reported measurements of 4.2 Sv. Similarly good agreement is found for the Hornbanki and Iceland-Faroe Ridge sections and for monitoring Atlantic Water outflow across the Barents Sea Opening to the Arctic shelf.

Citation: Hunegnaw, A., F. Siegismund, R. Hipkin, and K. A. Mork (2009), Absolute flow field estimation for the Nordic seas from combined gravimetric, altimetric, and in situ data, *J. Geophys. Res.*, *114*, C02022, doi:10.1029/2008JC004797.

1. Introduction

[2] The determination of the absolute ocean circulation is a major challenge in physical oceanography. The transport of water mass is connected to the transport of heat and salt, their budgets are key elements for understanding the ocean's role in the global climate system.

[3] The ocean circulation, on time scales of a few days or longer and spatial scales exceeding a few tens of kilometers, is basically in geostrophic balance of horizontal pressure gradients and the Coriolis force. The vertical change of the pressure gradient, and thus the depth-variable, baroclinic part of the flow, is via the thermal wind equation determined by horizontal density gradients, which in turn depend on the spatial distribution of water masses defined by their salinity and temperature. To determine the absolute flow the current velocity has to be known for a specific depth. In general this could be achieved by monitoring the mean current velocity at a specific depth. However, direct observation of current velocities is expensive. To obtain a realistic view on the spatial structure of the flow field (down to few tens of kilometers or so) to allow for realistic flux estimates, and to resolve temporal fluctuations, including seasonal variability, a dense array of instruments has to be operated for a period of several months to years. This is only affordable at some dedicated key locations. The traditional way to overcome the lack of direct current velocity observations applies the questionable assumption of a level of no motion [*Wunsch and Gaposchkin*, 1980]. The flow field implied by the method fails to conserve mass and violates other physical laws [*Wunsch and Stammer*, 1998].

[4] To overcome the problem of underdetermination, inverse methods are often used. Here a model is defined which, in addition to the thermal wind equation, can include conservation properties and further dynamical constraints, as well as additional data. The data as well as the model are allowed for errors. Estimates of the errors have to be provided. The inverse of the error is used to weight the misfit between the model and the data. In some cases a covariance information is also used. The solution of the inverse problem

[1] School of GeoSciences, University of Edinburgh, Edinburgh, UK.
[2] Nansen Environmental and Remote Sensing Center, Bergen, Norway.
[3] Now at Center for Marine and Atmospheric Science, Institute of Oceanography, University of Hamburg, Hamburg, Germany.
[4] Bjerknes Centre for Climate Research, Bergen, Norway.
[5] Also at Institute of Marine Research, Bergen, Norway.

0148-0227/09/2008JC004797

is then given by the minimization of the weighted model to data misfit. For a comprehensive introduction to the method and references, see, e.g., *Wunsch* [2006].

[5] Alternatively, a geodetic technique can be used to determine the absolute geostrophic current at the surface. This geostrophic surface current can be determined by the slope of Dynamic Topography (DT). The DT, ζ, is observed as the difference of altimetric sea surface height, h and the geoid, N, a reference equipotential surface of gravity field. Usually the mean DT (MDT) for a given time period is requested. The relationship of the time mean quantities is then given by

$$\overline{h} = N + \overline{\zeta} \tag{1}$$

The MDT, $\overline{\zeta}$ usually differs from the geoid N with magnitudes in the range from 0.1 to 1 m over distances around 100 km. While the time-averaged mean sea surface height (MSSH) $\overline{h}$ is known with high accuracy of few centimeters [e.g., *Wunsch and Stammer*, 1998; *Chelton et al.*, 2001; *Tapley and Kim*, 2001; *Andersen et al.*, 2003; *Rio and Hernandez*, 2004], existing global geoid models, based on a combination of terrestrial and spaceborne gravimetry, have hitherto not provided an accuracy better than several tens of centimeters [*Johannessen et al.*, 2003]. The precise calculation of the MDT using mean sea surface height and geoid information had therefore not been possible at this wavelength, so that uncertainties in transport estimation remained [*Wunsch and Stammer*, 1998].

[6] Because of the large uncertainties in the geoid models, global MDT estimates have not so far incorporated local or regional-scale geoid information. Large improvements in the determination of the MDT are expected after the launch of the European Space Agency (ESA) Gravity field and steady state Ocean Circulation Explorer (GOCE) satellite mission. When combined with precise satellite altimetry, the accurate ($\approx$1 cm) and high-resolution ($\approx$100 km) marine geoid that GOCE aims to observe will enable new estimates to be made of MDT. In combination with in situ data and ocean models, this will provide a much needed high-resolution window on the ocean circulation at depth, as elaborated by *Johannessen et al.* [2003] and *Knudsen et al.* [2006].

[7] However, for some regions, a large number of surface gravity observations already exists. Together with longer-wavelength information from the Gravity Recovery and Climate Experiment (GRACE), they can be used to estimate a regional-scale geoid with the accuracy needed to estimate the MDT. The benefit is twofold: First, the "geodetic" MDT contains new valuable information about the ocean dynamical system and, second, the geoid might serve as reference for calibration or validation of GOCE gravimetric data.

[8] Here we concentrate in the Nordic seas. The region is unique in the sense that there is an unusually dense coverage of gravimetric data, and that a large number of in situ temperature and salinity observations is available. A three-dimensional flow field is estimated from this data source: The surface current is derived from the geodetic MDT while the dependence of the circulation on depth is determined from the hydrographic database.

[9] The geodetic based MDT comes from modifying an initial "first-guess" regional MDT model in two steps: first, we make its long-wavelength structure consistent with satellite altimetry, combined with the reliable parts of the geoid as deduced from GRACE observations; secondly, we add shorter-wavelength information coming from surface gravity data. On closer examination, the second task is neither linear nor independent, making a simple application of equation (1) misleading.

[10] The problem is not an evaluation of equation (1) to obtain an optimal estimate of the two independent quantities from observations of all three because the geoid is not an observable. Computing a gravimetric geoid, N involves a surface integral of gravity, meaning that gravity coverage must be complete. Consequently, practical evaluation requires gravity to be interpolated into the gaps between survey lines. *Hunegnaw and Hipkin* [2006] and *Hunegnaw et al.* [2009] describe how ship and airborne gravity data were cleaned and adjusted to provide a strong constraint for surface gravity along survey lines. The interpolation process is then done by our algorithm called the iterative combination method (ICM) (section 2.3). It generates complete grids of gravity and MDT that are mutually consistent.

[11] Section 2 first introduces the numerical methods we use in section 2.1 and then the observational data used to quantify the part of the flow field driven by water density (section 2.2) and the geodetically determined part of the flow (section 2.3). This is followed by a description of the drifter data used for an alternative estimate of surface flow that we need for validating the ICM MDT (section 2.4).

[12] The validation is presented in section 3. The ICM MDT is compared to other MDT estimates derived from hydrodynamic modeling. Those models were used as initial MDTs in the ICM (see section 2.3). The comparison to those models aims to estimate the sensitivity of the ICM MDT to the initial field. This is an important issue since it determines to what extent the gravimetric and altimetric data used in the ICM adds information to the modeled MDTs or, in other words, to what extent the final MDT is independent from the a priori model. This comparison thus indicates to what extent oceanography can benefit from including gravimetric data when synthesizing the DT (see section 3.2). In section 3.3 we validate the surface geostrophic flow field as derived from the ICM MDT with independent, drifter data.

[13] To determine the flow field below the sea surface salinity and temperature observations extracted from the Norwegian Iceland Seas Project (NISE) [*Nilsen et al.*, 2008] database are used to determine the baroclinic part of the flow (see section 2.2). The NISE data set is based on data from the ICES database (http://www.ices.dk/) together with data from the Arctic and Antarctic Research Institute (AARI) in Russia, Institute of Marine Research (IMR) in Norway, Marine Research Institute (MRI) in Iceland and the Faroese Fisheries Laboratory (FRS). The resulting 3-D flow is compared with observed salt, heat and mass transport across key cross sections: the Barents Sea opening in section 4.2, the Svinøy section northwest from northern Norway in section 4.3; the Iceland-Faroes Ridge in section 4.4; the Hornbanki section northward from northwest Iceland in section 4.5, and the

Faroes-Shetland Channel in section 4.6. We discuss the results and the major conclusions in section 5.

2. Methods and Input Data

2.1. Absolute Geostrophic Currents

[14] On time scales longer than a few days, the large-scale (~100 km) ocean circulation is to a good approximation geostrophic. Geostrophic currents are calculated from

$$\mathbf{u} = \frac{1}{f\rho_0}\mathbf{k} \times \nabla p \tag{2}$$

with $\mathbf{u}$ the horizontal current velocity, $\mathbf{k}$ the vertical unit vector, the pressure p, ρ_0 the density and f the Coriolis parameter. The pressure at depth z_0 neglecting the surface air pressure is given by

$$p = g\int_{z_0}^{\zeta} \rho dz \tag{3}$$

and the horizontal pressure gradient as

$$\nabla p = g\rho_\zeta \nabla\zeta + g\int_{z_0}^{\zeta} \nabla\rho dz. \tag{4}$$

Here, ζ is the MDT, the height of the ocean surface above the geoid, ρ_ζ is the water density at the surface, and g the acceleration of gravity. With the approximation

$$\nabla p \approx g\rho_\zeta \nabla\zeta + g\int_{z_0}^{0} \nabla\rho dz \tag{5}$$

the first term on the right hand side of equation (5) is only dependent on the MDT, while the second term is only dependent on the density structure. There is no significant error so long as variations of ρ above the geoid can be neglected. Insertion of equation (5) into equation (2) gives

$$\mathbf{u} = \mathbf{u}_{surf} + \mathbf{u}_{bc} \tag{6}$$

with

$$\mathbf{u}_{surf} = \frac{g}{f}\mathbf{k} \times \nabla\zeta \tag{7}$$

and

$$\mathbf{u}_{bc} = \frac{g}{f\rho_0}\mathbf{k} \times \int_{z_0}^{0} \nabla\rho dz. \tag{8}$$

The slope in the MDT causes a horizontal pressure gradient that drives $\mathbf{u}_{surf}$. At depth, this pressure gradient may be modified by horizontal gradients in water density caused by the temperature and salinity distribution. The extra component of the current $\mathbf{u}_{bc}$, is density driven and called the baroclinic flow. It is zero at the surface, so $\mathbf{u}_{surf}$ is determined from our MDT, found from geodetic data using ICM. The modification of the flow with depth ($\mathbf{u}_{bc}$) is determined by hydrographic data from the NISE database.

2.2. Baroclinic Flow and the NISE Database

[15] Measurements of pressure, temperature and salinity were compiled for the Nordic NISE project, originally to describe the ocean climate variability and its link to fishery resources in the Nordic seas. The NISE compilation is based on data from the ICES database (http://www.ices.dk/), together with data from the Arctic and Antarctic Research Institute (AARI) in Russia, the Institute of Marine Research (IMR) in Norway, the Marine Research Institute (MRI) in Iceland and the Faroese Fisheries Laboratory (FRS). We used them to compute the baroclinic flow. Data earlier than the mid 1970s as well as the AARI data are from water samples and have a coarse vertical resolution. Nearly all the remaining profiles are high-resolution conductivity-temperature-depth (CTD) casts. The data are interpolated at 30 standard depths (0, 10, 20, 30, 50, 75, 100, 125, 150, 200, 250, 300, 400, 500, 600, 700, 800, 900, 1000, 1100, 1200, 1300, 1400, 1500, 1750, 2000, 2200, 2500, 3000, and 3500 m). Although the data set covers the entire Nordic seas and consists of about 300,000 profiles, observations were inhomogeneously distributed in space and time. Most were collected between 1950 and 1995, with the number of profiles peaking between 1984 and 1989 (Figure 1). Seasonally, most hydrographic stations were recorded in June (more than 55,000 (19% of the total), and the fewest in December (about 10,000 stations, 3% of the total). The southern Norwegian Sea had the best spatial coverage and there were no profiles at all in the ice-covered east coast of Greenland.

[16] The analysis of the temperature and salinity observations in the NISE database started by computing the density [*Fofonoff and Millard*, 1983]. All density, temperature and salinity profiles were linearly interpolated to the standard depths as defined above. Profiles with missing data for three standard depths or more are discarded. For every standard depth, the three hydrographic parameters are binned to the 15' longitude × 5' latitude grid using a Gaussian low-pass filter with a width at half-peak amplitude of 59 km (standard deviation σ = 25 km). The gridded density field is then used to calculate $\mathbf{u}_{bc}$ according to equation (8).

2.3. Geodetic Data and the Iterative Combination Method

[17] The coverage of ship-based gravity surveys in the Nordic seas is amongst the densest in the world (see Figure 2). In addition, long, transoceanic flight lines on a recent airborne gravity survey have strengthened the marine data. Nevertheless, the gravity power spectrum increases rapidly with wavelength, so a complete geoid cannot be found with surface data alone: the longest wavelengths need further constraint. We generated composite free air gravity anomalies Δg by fitting terrestrial data to the very long wavelength part of the GRACE global gravity field model [*Tapley et al.*, 2004]. *Hunegnaw and Hipkin* [2006] and *Hunegnaw et al.* [2009] describe a novel approach of cleaning the raw gravity data and then using a network adjustment to minimize crossover errors. This resulted in very well controlled gravity data but only along survey tracks.

[18] The adjustment demonstrated that, at shorter wavelengths, surface data are inherently accurate enough to meet the geoid target of a few centimeters needed for

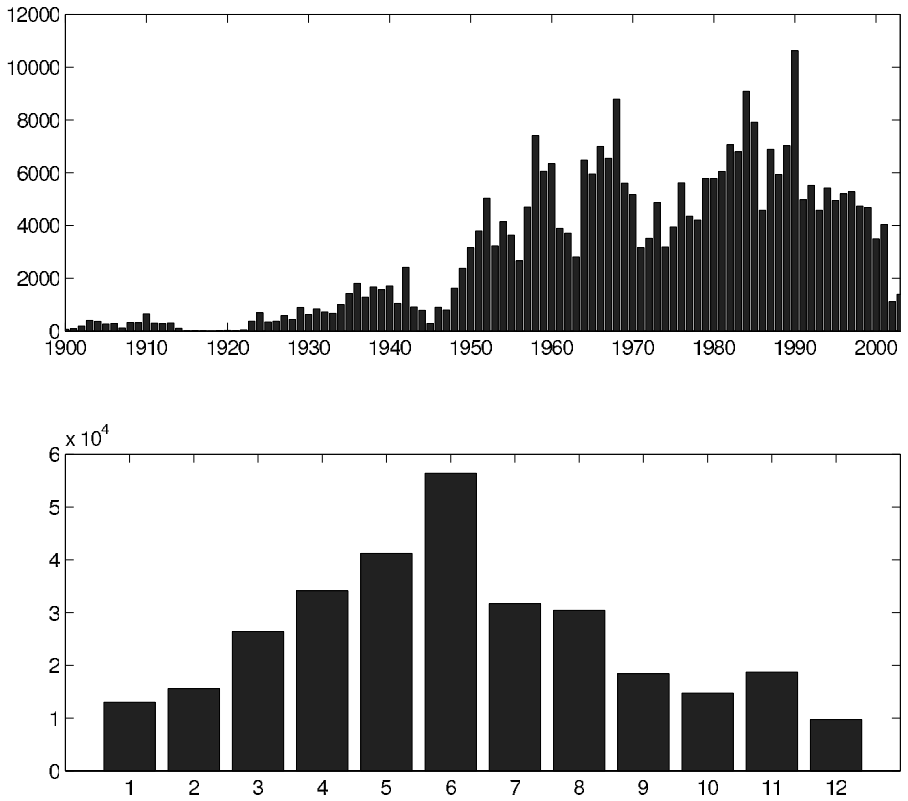

Figure 1. (top) Annual and (bottom) monthly distribution of profiles in the NISE database. The vertical scale gives number of profiles.

oceanographic applications. However, their coverage is not complete. Empirical interpolation into the data gaps between survey tracks generated gross geoid errors with unrealistic bumps many decimeters in size. The alternative approach is to fill in the gaps between survey lines with synthetic gravity generated from sea surface altimetry. This approach effectively approximates equation (1) by ignoring MDT or replacing it by an a priori long-wavelength model. We have developed a more rigorous way to use the available information called the iterative combination method (ICM) [*Hipkin and Hunegnaw*, 2006].

[19] The ICM approach combines three data streams: (1) gravity anomalies, Δg, determined with high accuracy by our cleaning and adjustment algorithms but only available

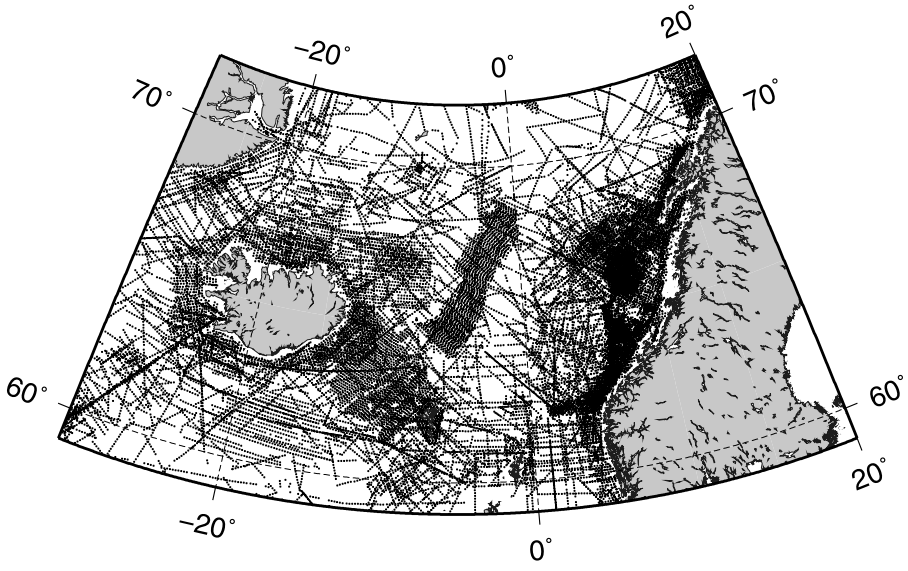

Figure 2. Marine gravity data in the Nordic seas, thinned to an along-track distance of 10 km.

along survey lines; (2) satellite altimetry giving an effectively complete coverage of MSSH, h; and (3) an initial MDT model, ζ, derived from a global ocean circulation model. Bruns equation [*Heiskanen and Moritz*, 1967]

$$N = -\frac{T}{\mathrm{g}} \tag{9}$$

relates the geoid height N to the anomalous gravity potential T. In the short-wavelength limit (wavelengths much less than 2000 km)

$$\Delta \mathrm{g} \approx -\frac{\partial T}{\partial z} \equiv \mathrm{g}\frac{\partial N}{\partial z} \tag{10}$$

Because the gravity potential satisfies Laplace's equation, its variation with height is related to its horizontal derivatives and they are observable. The notation $\frac{\partial N}{\partial z}$ should be understood via equation (10). We treat MSSH, h and MDT ζ, as they were derived from a potential in the same way as N, also determining their ''vertical derivative'' from the observable behavior over the horizontal surface.

$$\Delta \mathrm{g}_{obs} \approx \mathrm{g}\frac{\partial N}{\partial z} = \mathrm{g}\frac{\partial h}{\partial z} - \mathrm{g}\frac{\partial \zeta}{\partial z} = \Delta \mathrm{g}_{PS} - \mathrm{g}\frac{\partial \zeta}{\partial z} \tag{11}$$

The first term on the right hand side of equation (11) is what some call the ''altimetric gravity anomaly.'' We prefer the name ''pseudo–gravity anomaly,'' although our use of the name is looser than the one coined by *Baranov* [1957]: he introduced it for a gravity anomaly proxy computed from magnetic observations. A name with the prefix ''pseudo'' emphasizes that our ''pseudo–gravity anomaly,'' $\Delta \mathrm{g}_{PS}$, is, like Baranov's version, not real gravity but a proxy for it. The second term shows that the bias of the ''pseudo–gravity anomaly'' corresponds to the gravity effect derived from the MDT. For oceanographic purposes, the systematic difference between $\Delta \mathrm{g}_{PS}$ and the real gravity anomaly Δg is crucial. Computing the difference from oceanographic estimates of MDT shows that it reaches $\sim$2 mGal (1 mGal = 10^{-5}m s^{-2}) and appears to be dominated by wavelengths longer than 100 km. However, both its apparent smoothness and its limited amplitude may be a spurious consequence of the low resolution of oceanographic models. The spectral characteristics of real MDT are not well known.

[20] Physical geodesy normally uses the inverse of equation (9), which implicitly uses Laplace's equation to replace a derivative or integral over the vertical coordinate z by horizontal derivatives or an area integral over the horizontal surface

$$\mathrm{N} = \int\int F \Delta \mathrm{g} ds \tag{12}$$

F is a kernel function relating a gravity anomaly at one point to its geoid contribution at another [see *Heiskanen and Moritz*, 1967]. In equation (12) we can substitute either a real gravity anomaly for Δg, or a synthetic version derived from the two terms on the right-hand side of equation (11), or a weighted combination of the two. The weighted combination allows us to create a complete grid of gravity anomalies so that equation (12) gives a complete grid of geoid heights.

[21] The process, which has to be iterative because ζ is initially unknown and the quantity being sought, is described by

$$h - \zeta_{i+1} = \int\int F \left[\frac{w_G \Delta \mathrm{g} + w_A \mathrm{g}\left(\frac{\partial h}{\partial z} - \frac{\partial \zeta_i}{\partial z}\right)}{w_G + w_A} \right] ds \tag{13}$$

We start by using an initial estimate for ζ derived from a global circulation model for the right hand side of equation (13) to get a revised estimate of MDT on the left-hand side. Equation (13) represents this iterative loop that continues until the interpolation of gridded gravity on to the survey tracks adequately reproduces the measured along-track gravity. Integration and differentiation use a Fast Fourier Transform (FFT) technique.

[22] Here, the altimetric sea surface h is considered known. We have used the CLS01 [*Rio and Hernandez*, 2004] MSSH model, adjusted for the time average for the period 1993–1999. The routine uses two grids of weights. The altimetry weight, w_A, is set to zero on land and unity over the oceans with a smooth transition over the coastline. The surface gravity weight, w_G, is unity on land but offshore, it is assigned a value that decreases rapidly away from survey tracks. w_G is computed at each grid point as the sum of a contribution from every marine or airborne gravity observation. Each contribution decreases with distance from the observation point in a way that matches the gravity effect of a point mass within the upper crust. These contributions are scaled by the standard deviation of the survey data along each survey line [*Hunegnaw and Hipkin*, 2006; *Hunegnaw et al.*, 2009].

[23] The ICM algorithm has two equivalent outputs: a grid of final MDT values and a grid of composite gravity anomalies. The iterative scheme converges rapidly, with a good solution after a couple of iterations. After 10 iterations, the RMS incremental change per iteration in the MDT model over the Nordic seas is less than 3 mm; the corresponding change in gravity anomaly is less than 0.04 mGal. The routine was tested initially using a composite MDT. This MDT had been derived from a weighted combination of four oceanographic and two other observational estimate models [*Bingham and Haines*, 2005].

[24] The ICM MDT was computed on a high-resolution grid (2' longitude $\times$ 1' latitude) as shown in Figure 3. Before calculating the surface current from it, values on land (due to FFT edge effects) were blanked out using a land mask and the ICM MDT has been smoothed with a Gaussian low-pass filter with a width at half-peak amplitude of 59 km (σ = 25 km) to reduce noise generated from differentiation. Still its resolution is better than that anticipated from the satellite based GOCE mission. Finally, the flow was binned to the lower 15' longitude $\times$ 5' latitude grid used in the study. We compute the two components in equation (6) separately: the surface flow from ICM MDT with equation (7), the baroclinic effect at depth using the NISE database with equation (8). Finally the filtered ICM MDT together with

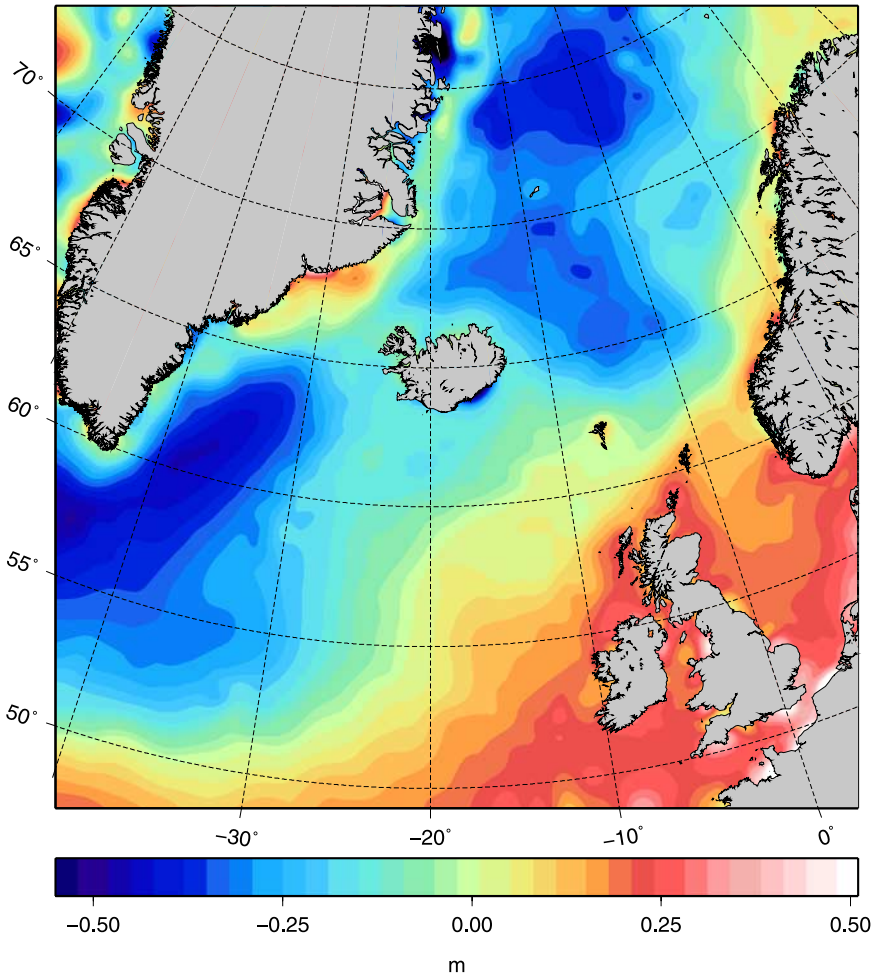

Figure 3. The ICM MDT model, smoothed with a Gaussian low-pass filter σ = 25 km.

the interpolated and filtered hydrography gives an integrated product that describes the three-dimensional total flow field.

2.4. Drifter Data

[25] Drifter buoy data in the Nordic seas were collected by the World Ocean Circulation Experiment–Tropical Oceans Global Atmosphere (WOCE-TOGA) Surface Velocity Program (SVP). They give instantaneous water displacement directly [*Niiler et al.*, 1995]. Most drifters in the Nordic seas were deployed in three regions: the Iceland Plateau north of Iceland; the Iceland-Faroe Front east of Iceland, and over the Norwegian Coastal Current. Drifters consist of a drogue at a depth of 15 m tethered to a surface float [*Sybrandy and Niiler*, 1990]. The direct influence of wind and waves on the drifters, as well as Ekman drift and measurement errors, are neglected. Motion of the drogue due to wave and wind drag on the buoy is estimated to be less than 0.1% of the wind speed [*Niiler and Paduan*, 1995]. In the Nordic seas, Ekman drift is small compared to the geostrophic flow [*Jakobsen et al.*, 2003].

[26] In this paper, we have used temperature, time and position from 1180 drifters over the period 1990–2006. The time series from which we deduced currents had been quality controlled and optimally interpolated as follows: outliers were removed by a despiking program and the result interpolated at 2-h intervals [*Hansen and Poulain*, 1996]; high-frequency components due to tidal and inertial currents were suppressed with a 36-h low-pass filter [*Otto and van Aken*, 1996]; these data were thinned to a 6-h subsample (http://www.aoml.noaa.gov). For our analysis, we additionally suppressed mesoscale variability by Gaussian smoothing as an 18-day low-pass filter. Figure 4a (Figure 4b) shows the motion of drifter 15925 over the Iceland-Faroe Front between February 1993 and August 1994 before and after our filtering. To estimate the mean flow, velocities were averaged into 1° latitude by 2° longitude bins and located at the center of the bin, as in the work by *Jakobsen et al.* [2003].

2.5. Ocean General Circulation Models

[27] The "first-guess" MDT used for the ICM algorithm was initially a composite model called CMDT, produced by averaging six MDT estimates, most derived by assimilating direct observations of the ocean state into dynamic ocean circulation model: (1) the CLS (Collecte, Localisation, Satellites) combined mean dynamic topography model Rio03 [*Rio and Hernandez*, 2004]; (2) FOAM, an operational ocean model used by the U.K. Meteorological Office (http://www.metoffice.com/research/ncof/foam/index.html); (3) OCCAM (Ocean Circulation and Climate Advanced Modelling) [*Saunders et al.*, 1999]; (4) the DIADEM assimilation by the Nansen Institute; (5) ECCO (Estimating the

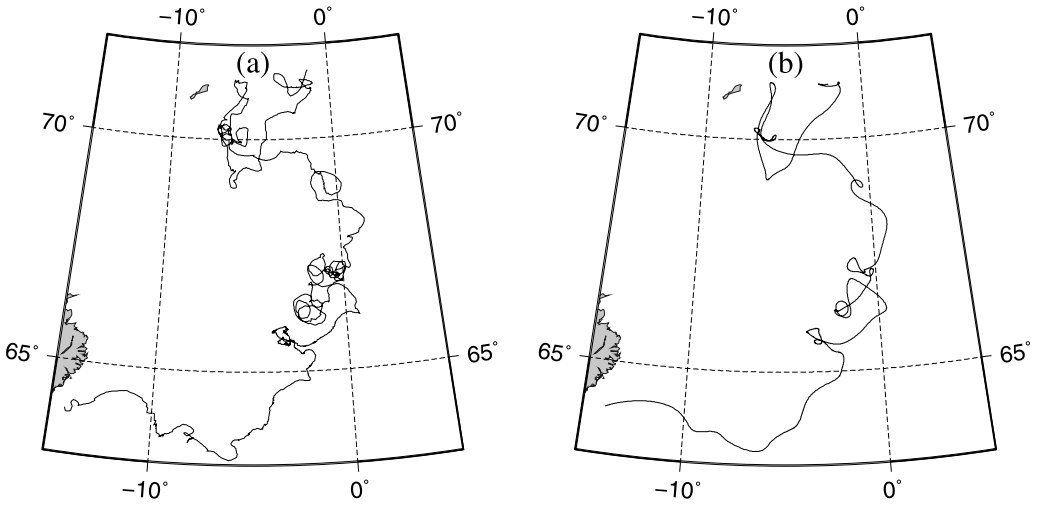

Figure 4. (a) Trajectory of the original drifter 15925 and (b) filtered with 18-day period.

Circulation and Climate of the Ocean) [*Köhl et al.*, 2007]; and (6) the Maximenko-Niiler MDT derived from a combination of satellite altimetry and 10 years of drifter data [*Maximenko and Niiler*, 2004]. When this composite model is used as the ICM "first guess," the output is called ICM CMDT. The initial MDT estimates were available on grids of different coordinates and with different resolutions: latitude and longitude grids for FOAM (spacing 1/3°); Rio03 (spacing 1/4°); OCCAM (1/4°); Maximenko-Niiler (0.5°), and ECCO (spacing 1°). DIADEM used a variable projected grid equivalent to 18 to 23 km. The ICM product comes on a 2 km grid of a Lambert's conical projection, to which all other models were smoothly interpolated.

[28] Differences between models were reduced to zero mean and smoothed with the same Gaussian low-pass filter (σ = 25 km). Statistical comparisons excluded onshore data and offshore grid points within 20 km of the coast: for the inshore region, uncontaminated altimetry may be sparse.

[29] Table 1 shows all differences between seven MDT models: ICM CMDT and the six initial MDTs that contributed to the CMDT. The smallest standard deviation of the mismatch with ICM CMDT is for Maximenko-Niiler (69 mm) and the largest is for FOAM (123 mm). Overall the smallest standard deviation (63 mm) is between ECCO and Maximenko-Niiler and the largest is between Rio03 and FOAM (148 mm). Thus the ICM CMDT is comparable with some of the best controlled ocean general circulation models (OGCMs). Figures 5a, 5c, 5e, and 5g compare each of the OGCMs with the CMDT chosen as reference dynamic topography.

3. Near-Surface Circulation

3.1. Overview

[30] Except for a small contribution from the wind-driven Ekman drift, large-scale long-term surface flow is described by the geostrophic equation (7). Consequently, predicted currents depend on the gradient of MDT, not MDT itself. However, both the input and output of the ICM algorithm involves MDT and geodetic quantities linked to it by equation (1), so every MDT model has been adjusted to a zero global mean before comparison or combination in order to avoid irrelevant differences.

3.2. Sensitivity of the ICM MDT

[31] The six oceanographic MDT models differ from each other with a standard deviation in the Nordic seas, averaging 110 mm and ranging up to 148 mm (Table 1). *Femke* [2007] has also made a comparison between several MDTs over the wold ocean. He found RMS differences that vary between 42 mm to 105 mm after low-pass filtering with an effective resolution of 167 km. Using the six oceanographic MDT models to initiate the ICM process produces outputs that differ from each other with a standard deviation of only 26 mm (Table 2). This means that the output of the ICM routine is rather insensitive to the "first-guess" model, implying that geodesy is adding real information to the OGCM. Figures 5b, 5d, 5f, and 5h show the difference in ICM output MDT for each input compared with that for the composite MDT input (ICM CMDT).

3.3. ICM Surface Circulation

[32] Figure 6a shows surface geostrophic currents predicted by the ICM CMDT. Figure 6b displays the time-averaged circulation for the period 1990–2006 derived from filtered Lagrangian buoy trajectories. The two methods give results that agree in the location of the strong currents along the western, southern and eastern margins of the Nordic seas. In particular, the two branches of the Norwegian Atlantic Current (NwAC) are reproduced in the flow deduced from the ICM CMDT, including the bifurcation of the western branch at 68°N. There, most of the water flows northward toward the Fram Strait but part of it follows the southern rim of the Lofoten Basin eastward toward the coast of Norway. We even see the small southward current at 7°W, approximately following the 2000 m isobath between the Iceland and the Norwegian Basins. Some ICM CMDT current velocities are lower than those observed from the drifter data because ICM CMDT is smoothed. Smoothing reduces locally steep slopes at boundary currents but spreads the same flow over a wider region. ICM CMDT fails to match the observed rate of the northeastward flow of North Atlantic Current through 18°W, 60°N toward the Iceland-Faroe Ridge, probably

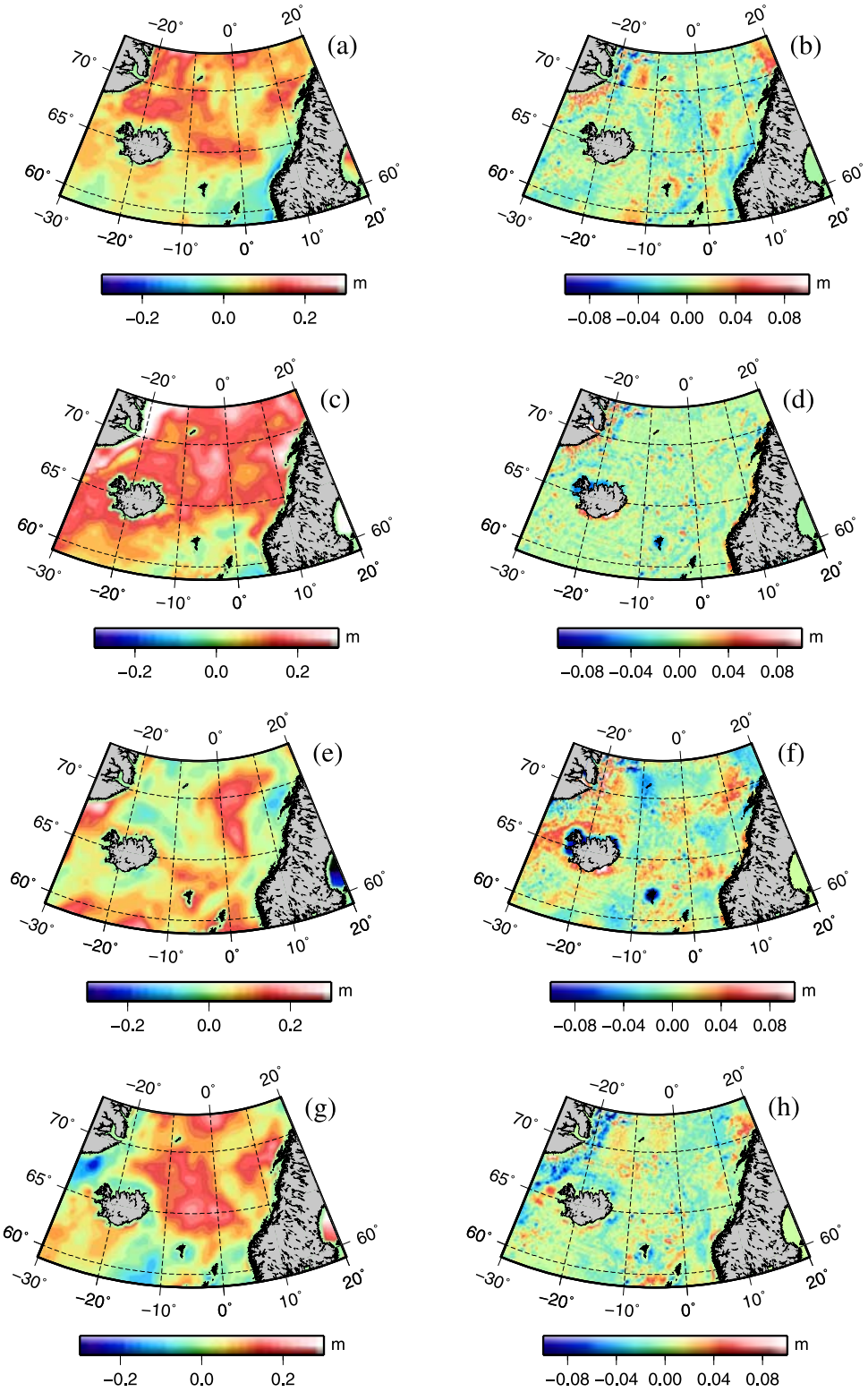

Figure 5. Spatial maps of the differences between the various MDT models ((a and b) Maximenko-Niiler, (c and d) OCCAM, (e and f) DIADEM, and (g and h) ECCO) and the reference CMDT (Figures 5a, 5c, 5e, and 5g) and ICM MDT solutions derived from different initial MDT models with respect to ICM CMDT (Figures 5b, 5d, 5f, and 5h). Note that the color scales differ by a factor of three.

Table 1. Standard Deviation of the Difference Between Various MDT Models[a]

Parameter	ICM CMDT	OCCAM	Rio03	FOAM	DIADEM	Maximenko-Niiler	ECCO
ICM CMDT		10.1	10.6	12.4	8.0	6.9	6.9
OCCAM	10.1		14.0	11.9	12.1	6.3	9.2
Rio03	10.6	14.0		14.8	14.1	12.5	12.8
FOAM	12.3	11.9	14.8		11.1	11.4	13.4
DIADEM	8.0	12.1	14.1	11.1		9.0	8.1
Maximenko-Niiler	6.9	6.3	12.5	11.4	9.0		6.2
ECCO	6.9	9.2	12.8	13.4	8.1	6.2	

[a]Unit is cm.

because of poorer gravity coverage there. However, the failure of ICM CMDT to detect the strong southward flow of drifters in the Greenland Sea at 10°W is probably due to a transient phenomenon, an interpretation supported by results from *Jakobsen et al.* [2003]: their drifter data for the period 1990–2000 did not find this feature [*Jakobsen et al.*, 2003, Figure 5]; otherwise their circulation map is very similar to ours derived from the extended drifter data set (Figure 6b).

[33] The ability of ICM CMDT to predict the velocity of drifting buoys was tested during a CLS validation experiment (M.-H. Rio, personal communication, 2005). The time averaged baseline of ICM CMDT currents were converted to instantaneous velocity estimates using current anomalies deduced from satellite altimetry. The CLS group compared this with 172920 observations of buoy velocities for the period from 1993 to 2003.

[34] The experiment has been repeated here with three MDT models for the mean flow: ECCO, Maximenko-Niiler, and the ICM CMDT. Table 3 shows the root-mean-square deviation of the east-west and north-south components of velocity difference, and a vectorial correlation coefficient (M.-H. Rio, personal communication, 2005). The ICM CMDT does better than the instantaneous MDT derived with an ECCO baseline, even though ECCO assimilates surface drifter data but, not surprisingly, the Maximenko-Niiler MDT performs best, because it is deduced directly from the drifter data.

[35] The technique described by *Rio and Hernandez* [2004] gave a further comparison to ICM CMDT velocities. They used a given MDT model as "first guess" to estimate an improved MDT in a multivariate objective analysis of altimetric height anomalies and buoy velocities. They synthesize a local MDT by subtracting oceanic variability as observed by satellite altimetry from the full dynamical signal based on buoy velocities from the WOCE-TOGA program and XBT, CTD casts [*Rio and Hernandez*, 2004]. Table 4 gives the same type of performance indicators as Table 3 but now for the year 2003 only. It compares the output of synthesized MDT (for the ICM CMDT input we call this ICM SMDT), with the three input models. ICM SMDT now correlates with observations as well as the Maximenko-Niiler model and has an RMS velocity misfit that is only 0.3% larger.

4. Depth-Integrated Transports

4.1. Overview

[36] Broad MDT lows (Figure 3) map out the Nordic seas gyre, the latter partially divided by higher MDT along the latitude of Jan Mayen Island, and the eastern lobe of the Labrador-Irminger Sea gyre. Boundary currents connecting the edges of the gyres are identified by steeper MDT gradients: the North Atlantic Drift and then the Norwegian Atlantic Current carry warm subtropical waters past the southeast margin of the Labrador Sea and then northward into the eastern side of the Nordic seas; the opposite direction, the East Greenland Current carries cold polar waters along the east and the southwestern coast of Greenland. The geostrophic velocity map (Figure 6a) gives some indication of the continuity of flow and how boundary currents interact with the gyre circulation but the NISE hydrographic data provide direct water mass markers as well as an extrapolation to depth. Consequently, we can now investigate properly the routes by which subtropical Atlantic Water or Polar waters infiltrate into the Nordic sea gyre and, in principle, quantify volume, salt and heat transport for each water type.

[37] In this section, we compare hydrographic observations with our estimate of volume, heat and salt transports through key cross sections in the Nordic seas (Figure 7): the Barents Sea Opening (BSO) crosses the eastward flow of the Atlantic Water on to the Arctic shelf and westerly flow of the Arctic waters into the Atlantic; the Svinøy section crossing the Norwegian Atlantic Current (NwAC); the Iceland-Faroe Ridge section runs north from the Faroes to intersect the inflow of Atlantic Water carried over the ridge, the Hornbanki section runs from the western Iceland northward along 22°W, again to investigate the Atlantic

Table 2. ICM MDT Solutions Derived From Different Initial MDT Models: Standard Deviation[a]

Parameter	ICM CMDT	ICM OCCAM	ICM Rio03	ICM FOAM	ICM DIADEM	ICM Maximenko-Niiler	ICM ECCO
ICM CMDT		2.2	3.1	2.7	2.1	2.1	2.1
OCCAM	2.2		3.4	2.7	2.8	2.7	2.8
Rio03	3.1	3.4		2.7	3.5	2.6	2.9
FOAM	2.7	2.7	2.7		3.2	2.2	2.4
DIADEM	2.1	2.8	3.5	3.2		2.9	2.7
Maximenko-Niiler	2.1	2.7	2.6	2.2	2.9		1.7
ECCO	2.1	2.8	2.9	2.4	2.7	1.7	

[a]Unit is cm.

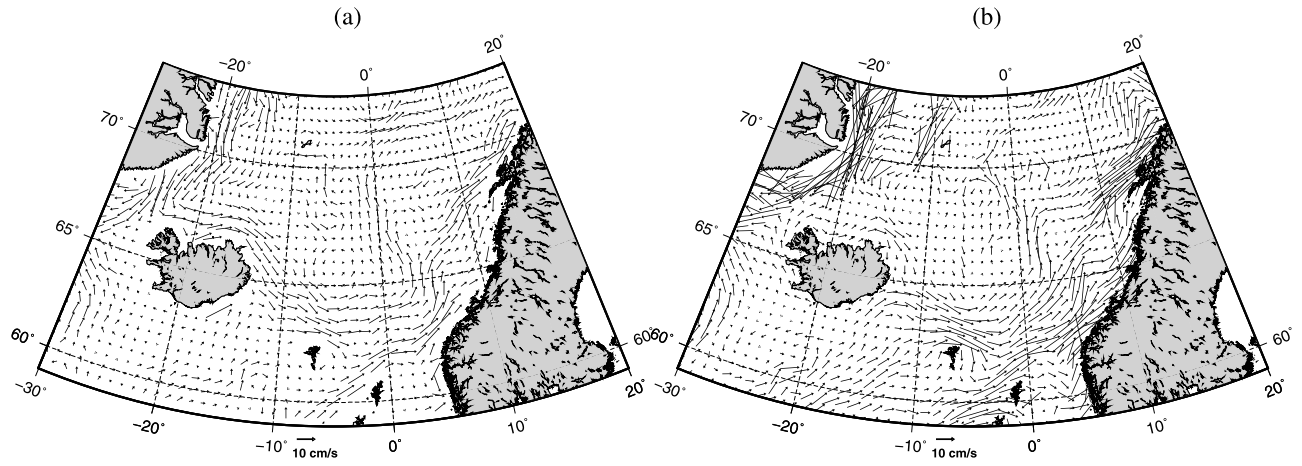

Figure 6. (a) The geostrophic currents as deduced from the final ICM CMDT and (b) currents deduced from Lagrangian drifters.

Water inflow, and the Iceland gyre circulation; finally the Faroe-Shetland Channel as important exchange route between the Atlantic and the Nordic seas. In order to ensure that the seasonal cycle could be resolved from the observations, we restricted our comparisons to places where either continuous observations were available from moored instruments lasting about a year or more, or regions with several cruises per year. Volume, heat and salt transports are summarized in Table 5. Where available we include direct measurements of current profiles in our comparisons.

4.2. Barents Sea Opening

[38] The cross section monitoring the Barents Sea Opening (BSO) runs 600 km north from Norway to Bjørnøya along 17°E.

[39] Estimates of time-averaged transports across the BSO section are reported by *Ingvaldsen et al.* [2004a, 2004b]. They used records between 1997 and 2001 from moored current meters, together with hydrographic measurements and additional moorings of shorter duration. The moorings covered a profile along the BSO between 71°15'N and 73°45'N and from 50 m depth to the bottom. For this part of the section, they found a mean Atlantic Water flux of 1.3 Sverdrup (Sv, $1\text{Sv} = 10^6\ \text{m}^3\text{s}^{-1}$), the same value that we find for the same area and the same condition for Atlantic Water ($T > 3°$). For the missing parts not covered by the moorings (the upper 50 m and the northern and southern ends of the BSO), *Ingvaldsen et al.* [2004a] estimated the Atlantic Water transports from other sources. Including the upper 50 m gave them 1.4 Sv, (the same as our estimate); including the whole BSO south of Bear Island gave 1.5 Sv (we get 1.4 Sv).

[40] Our cross section for the BSO (Figure 8a) has a very similar structure to the observed one from *Ingvaldsen et al.* [2004b] (not shown). Like *Ingvaldsen et al.* [2004b], we found two cores of maximum eastward velocity exceeding 3 cm s^{-1} in the surface flow. However, our deeper currents show a smoother transition to low values toward the bottom than theirs. In addition, our westward boundary current along the northern slope of the Bear Island Channel is less intense.

[41] For the water mass defined by $S > 35.0$, $T > 3.0$°C, *Skagseth et al.* [2008] report volume (heat) fluxes of 1.8 Sv (48 TW) for the period from 1993 to 2006. Our estimates are somewhat smaller: 1.5 Sv (31 TW). However, for this section, *Skagseth et al.* [2008] found a strong upward trend in volume (heat) flux of 0.1 Sv (2.5 TW) per year over their 12 year period. Since the CLS01 MSSH we used to determine the ICM MDT is an average for the period from 1993 to 1999, our results might not be comparable with the fluxes found by *Skagseth et al.* [2008]. We therefore recalculated the ICM MDT with a rereferenced MSSH using sea level anomaly data for the period from 1997 to 2006. The new heat transport we found (42 TW) is much closer to the *Skagseth et al.* [2008] value while the volume transport (2.2 Sv) is somewhat higher than that observed.

[42] In addition, the current of cold low-salinity Arctic water in the upper 100 m as indicated by *Blindheim* [1989] is completely missing. However, the observations of *Blindheim* [1989] reflect summer transports; because there are large monthly scale fluctuations, in the order of the mean flow, they might not be representative of a long-term mean.

[43] A possible reason having a good net flow across the BSO but underestimating both the inflow and outflow is a depression in real MDT near the northern end of the section which is not seen by the ICM MDT. Such a depression in the MDT would increase the barotropic part of both, the eastward near-surface Norwegian Atlantic Current as well as the westward slope current. Note that, for a flat bottomed ocean, the net barotropic transport over the section only depends on the sea level difference between the end points, so would not be affected by a depression in MDT. In our case, where the depth does vary, a depression in MDT above the

Table 3. Validation Results for Different Models of the Mean Flow[a]

Parameter	RMS East Velocity V_E (cm s^{-1})	RMS North Velocity V_N (cm s^{-1})	Vector Correlation Coefficient R_c
ICM CMDT	11.2	10.5	0.47
Maximenko-Niiler	11.1	10.4	0.50
ECCO	11.5	11.2	0.41

[a]M.-H. Rio (personal communication, 2005).

Table 4. Result of Combining a Geodetic Model ICM MDT With Synthetic Estimates of MDT, Compared With Other Models of the Mean Flow for the Year 2003[a]

Parameter	RMS East Velocity V_E (cm s^{-1})	RMS North Velocity V_N (cm s^{-1})	Vector Correlation Coefficient R_c
ICM SMDT	12.72	12.43	0.44
ICM CMDT	12.90	12.72	0.40
Maximenko-Niiler	12.76	12.32	0.44
ECCO	13.09	12.90	0.39

[a]M.-H. Rio (personal communication, 2005).

deep part of the Bear Island Trough would not significantly change the net transports because both the bathymetry and the current are symmetric.

4.3. Svinøy Section

[44] The Svinøy section runs toward northwest from the Norwegian coast at 62°N and cuts through the entire Atlantic inflow to the Norwegian coast (see Figure 7). Both branches of the Norwegian Atlantic Current cross the section: the western branch (labeled NwAC-w in Figure 7) following the Arctic Front and the eastern branch following the continental slope (the Norwegian Atlantic Slope Current, NwASC). Previously, current meter moorings [*Orvik et al.*, 2001] have been only available to give transports for the eastern branch. Estimates for the western branch have mainly been based on hydrographic observations, assuming geostrophy and prescribing a level of no motion [*Mork and Blindheim*, 2000]. The ability of the ICM MDT to detect the western branch is therefore very significant but we nevertheless concentrate on the eastern branch for a comparison with observations. *Orvik et al.* [2001] and *Orvik and Skagseth* [2003] analyze current meters deployed on the Svinøy section for the period April 1995 to February 1999. They assume no flow west of 3°23'E, the western end of their meter deployment, and extrapolate the observed currents from the eastern end of the observations toward the Norwegian coast. They estimate a northward transport of Atlantic Water (S > 35.0, T > 5.0°C) of 4.2 Sv. We found a transport of 3.9 Sv east of 3°23'E. Since in our case the northward transport in the eastern NwAC branch extends to approximately 2.8°E (Figure 7) we calculated the transport for the enlarged section and found 4.3 Sv volume flux for the total branch. Thus our estimates agree quite well with observations.

[45] The structure of our flow across the section (Figure 8b) is similar to *Orvik and Skagseth* [2005]. West of the eastern branch, we found a deep countercurrent of core velocities exceeding 5 cm s^{-1} [*Nøst and Isachsen*, 2003] and a rather broad western branch of the NwAC at the surface with maximum velocity somewhat higher than 10 cm s^{-1} at longitudes approximately 0.5–2°E [*Mork and Blindheim*, 2000].

4.4. Iceland-Faroe Ridge

[46] For the section labeled "IFR" in Figure 7 and crossing the northern flank of the Iceland-Faroe Ridge (IFR), we compare our results with the observations made by *Hansen et al.* [2003], who used instruments moored along this profile. They combined acoustic Doppler current profiler (ADCP) measurements for the period from June 1997 to June 2001 with decade-long CTD observations to determine the total water volume flux and the amount of Atlantic Water flowing eastward through this section. Their

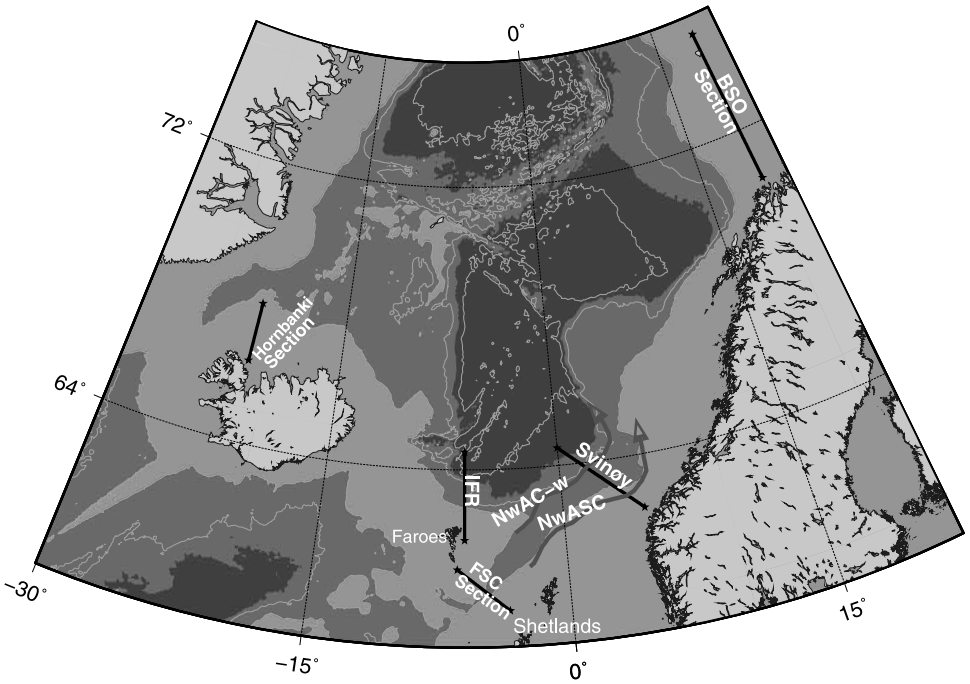

Figure 7. Schematic plots of the sections (solid lines). The Barents Sea Opening (BSO), the Svinøy, the Iceland-Faroe Ridge (IFR), the Hornbanki, and the Faro-Shetland Channel (FSC) sections and pathways of the Norwegian Atlantic Current: the western branch (NwAC-w) and the Norwegian Atlantic Slope Current (NwASC).

Table 5. Atlantic Water Mass (U), Salt (S), and Heat (H) Transport Estimates for Key Sections in the Nordic Seas From ICM MDT/NISE and Observations[a]

	ICM MDT + NISE	Observed	Citation
BSO, T > 3°C	U = 1.4 Sv	U = 1.5 Sv	*Ingvaldsen et al.* [2004a, 2004b]
BSO, z < 200 m, T > 2°C, S > 34.9	U = 1.2 Sv	U = 1.6 Sv	*O'Dwyer et al.* [2001]
	H = 26 TW	H = 39 TW	
	S = 41.10^6 kg s^{-1}	S = 57.10^6 kg s^{-1}	
Svinøy section, S > 35.0, T > 5°C	U = 3.9 (4.3) Sv	U = 4.2 Sv	*Orvik et al.* [2001], *Orvik and Skagseth* [2003]
Iceland-Faroe Ridge, S > 35.05	U = 2.9 Sv	U = 3.4 Sv	*Hansen et al.* [2003]
	H = 78 TW	H = 111 TW	
	S = 101.10^6 kg s^{-1}	S = 123.10^6 kg s^{-1}	
Hornbanki section	U = 0.95 Sv	U = 0.75 ± 0.15 Sv	*Jónsson and Valdimarsson* [2005]
Faroe-Shetland Channel, θ > 6°C, net northward flow	U = 3.5 Sv	U = 3.2 Sv	*Turrell et al.* [2003]
	H = 121 TW	H = 123 TW	
	S = 124.10^6 kg s^{-1}	S = 115.10^6 kg s^{-1}	

[a]Only long-term observations are included. For details see text.

result uses a three-point mixing model but they list also flux estimates for different reference salinities and temperatures [see *Hansen et al.*, 2003, Table 4].

[47] For the water mass defined by a salinity above 35.05, they find an eastward flow of Atlantic Water of 3.4 Sv (compared with 3.5 Sv for their three-point model). Their heat and salt flux are 111 TW and 123 × 10^6kg s^{-1}. We get transports of volume, 2.9 Sv, and salt, 101 × 10^6kg s^{-1} that are slightly smaller in about approximately the same proportion. However, our estimate of heat flux is very significantly smaller, only 78 TW.

[48] Since we find no substantial difference in the hydrography compared to *Hansen et al.* [2003], our lower heat transports imply too low a transport of warm near-surface water near the Faroe coast. Our velocity field (not shown) on the section (see Figure 7) is structurally very similar to *Hansen et al.* [2003, Figure 14] (not shown) although our total volume transport in the upper 600 m between 62°25'N and 63°35'N (4.1 Sv) is lower than the observed one (5.0 Sv). The essential difference is that our results give much smaller velocity over the steep slope of the Faroe Plateau: *Hansen et al.* [2003, Figure 14] shows core velocities at the surface of more than 22.5 cm s^{-1} and near bottom velocities larger than 10 cm^{-1} inshore of the 400 m isobath; our core velocity is only half (11 cm s^{-1}) and near bottom velocities hardly reach 5 cm s^{-1}. Our smaller fluxes might reflect the ICM CMDT having too small a gradient over the slope of the Iceland Plateau. A larger gradient would increase the eastward barotropic flow. Since comparably warm water is found above the steep slope, enhancement of the volume transport could increase the heat flux, making it more consistent with the estimates of *Hansen et al.* [2003].

4.5. Hornbanki Section

[49] The most western branch of Atlantic Water entering the Nordic seas passes northward through the Denmark Strait as the North Icelandic Irminger Current. It follows the western coast of Iceland into the Iceland Sea, and turns east to pass through the southernmost part of our Hornbanki section. This section runs north across the Icelandic shelf from the western end of Iceland (Figure 7). In our interpretation, it also extends across the eastward limb of the Iceland Sea gyre, through the low point of the associated MDT and then into part of the return westward flowing limb of the gyre. *Jónsson and Valdimarsson* [2005] deployed current meters on this section for the period 1994–2000. They estimated the fraction of the Atlantic water transported through the section from CTD measurements as well as additional hydrographic data upstream. They estimated Atlantic Water flow through the upper 200 m of the section between 66° 20'N and 67° 20'N averaging 0.75 Sv but very variable, with a further eastward flow of non-Atlantic Water of 0.38 Sv (one third of the total of 1.3 Sv). For the same section, we found 1.4 Sv of total eastward transport. Whether we use their estimate of the fraction of Atlantic Water, resulting in 0.95 Sv of Atlantic Water, or compare the total flow, our transports are slightly larger than theirs. In our section, the eastward flow at the surface extends to 67° 30'N. The flow is largely barotropic on the section (see Figure 8c) so net transport is mainly determined by the slope in the MDT. The shift in our current structure compared with *Jónsson and Valdimarsson* [2005] translates directly to a more northerly center of the ICM CMDT low and a larger area of eastward flow.

4.6. Faroe-Shetland Channel

[50] Several authors have reported transport estimates for the Faroe-Shetland Channel (FSC) [*Saunders*, 1990; *Isachsen et al.*, 2007; *Turrell et al.*, 2003; *Østerhus et al.*, 2005; *Hughes et al.*, 2005]. We concentrate on the results reported by *Turrell et al.* [2003] because their ADCP moorings and CTD observations are the longest continuous time series available, covering for the period 1994–2000. Identifying how much Atlantic Water comes directly northward through the Channel into the Nordic seas is complicated because there is also some Atlantic Water traveling eastward along the northern side of the IFR that recirculates in the channel. *Turrell et al.* [2003] identify surface Atlantic Water flowing directly into the Nordic seas as water with a potential temperature Θ > 6.0°C. They calculate a net Atlantic Water transport of 3.2 Sv averaged over the 6 year period, transporting 123 × 10^{12} W of heat and 115 × 10^6 kg s^{-1} of salt. On the same section and with the same constraint on the temperature, we found very similar values: a net northward volume transport of 3.5 Sv and heat and salt fluxes of 121 × 10^{12} W and 124 × 10^6 kg s^{-1}, respectively. *Østerhus et al.* [2005] report an import of 3.8 Sv for the period 1999–2001 on the same section. While the small difference in the results from different observations could indicate interannual variability influencing averages over different time periods or uncertainties in the method, our

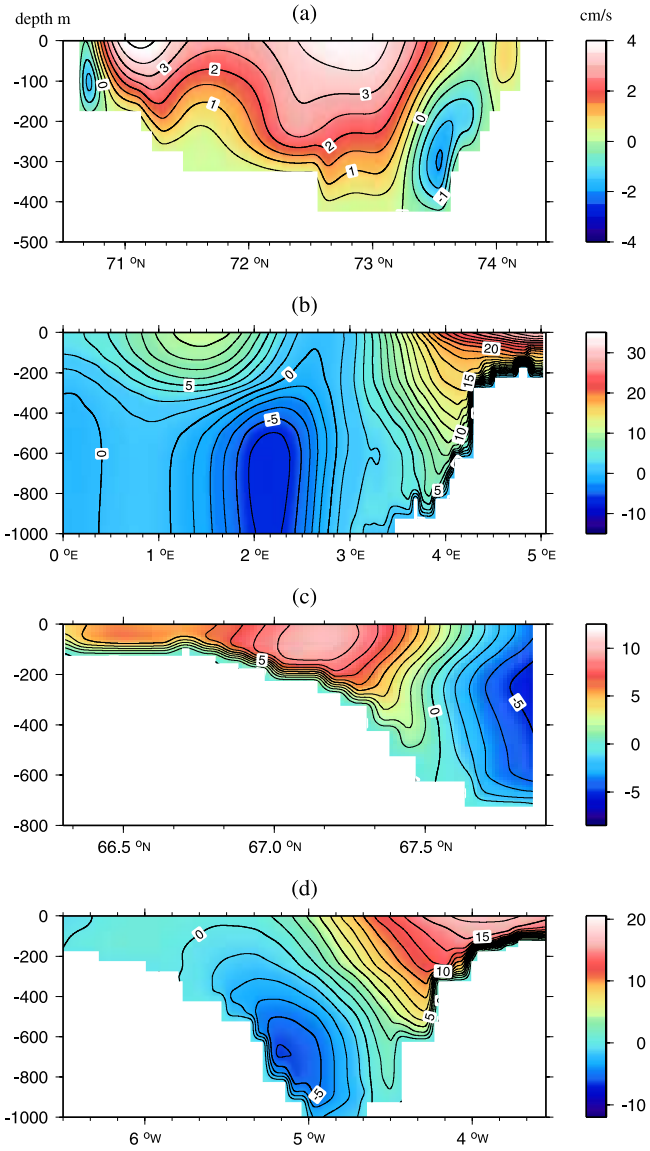

Figure 8. Modeled velocity in cm s^{-1} (a) across the BSO, (b) across the Svinøy (positive northward), (c) across the Hornbanki (positive eastward), and (d) across Faroe-Shetland Channel(positive northeastward) sections. See Figure 7 for the position of the sections.

results are in the range of uncertainty in the fluxes estimated from direct observations.

[51] Note, however, that *Turrell et al.* [2003] report a total southwestward flow of Atlantic Water (out of the Norwegian Sea) of 1.0 Sv while we found only 0.08 Sv. The velocity field on the section is displayed in Figure 8d. For both our and Turrell et al.'s results, the much stronger strong flow to the northeast into the Norwegian Sea is found toward the top of the bathymetric slope on the Shetland side of the Channel, while the flow out to the southwest is found in the deep central part and to the west. However, our core of flow to the southwest is found above the 800 m isobath on the slope of the Faroes Plateau rather than in the center of the channel. In general, *Turrell et al.* [2003] found a southwestward flow over the slope of the Faroe Plateau. Their flows indicate a minimum of the MDT low above the deepest part of the channel, at about 5°W, with a moderate MDT slope up toward the Faroes and a much steeper one up toward Shetland. In comparison the ICM MDT displays an upward slope on the southeastern part of the channel, but not as steep as expected from Turrell et al.'s model; however, the depression at 5°W is missing and the ICM CMDT is rather flat to the coast of the Faroes. Some differences in the temperature and salinity fields also contribute to the shifted position of the deep core of flow to the southwest.

5. Discussion

[52] In this study we have described a new algorithm called the iterative combination method (ICM) [*Hipkin and Hunegnaw*, 2006] and used it to compute an absolute mean dynamic ocean topography from marine gravimetry combined with satellite gravimetry and altimetry. Although the ICM algorithm uses a "first-guess" MDT derived from oceanographic models, the output is insensitive to which model is chosen, and becomes therefore an essentially geodetic product. This is then one of the first cases where using marine gravimetry to recover basin-wide details of current flow has achieved a precision that is useful to oceanography.

[53] In the Nordic seas between 59°N and 73°N, MDT has a range of about 50 cm and a standard deviation of less than about 20 cm. Inconsistencies between existing oceanographic MDT models are not small compared with this range. We compared six of them, most derived by assimilating direct observations of the ocean state into a dynamic ocean circulation model. The root mean square difference in the spatial structure of any two ranged from 14.8 cm to 5.2 cm. Using these models as the "first guess" for the ICM algorithm gave different ICM MDT models. The RMS difference between any two of these outputs ranged from 3.5 cm to 1.7 cm, much smaller than either the discrepancies in the first-guess MDTs or the spatial variability of MDT itself. Geodesy is contributing new information. Although this demonstrates that the ICM output is stable and consistent when primed with different oceanographic starting models, it does not show whether the product or any of the inputs matches reality.

[54] MDT uniquely determines geostrophic flow near the surface without reference to hydrographic data but does not determine flow driven directly by the wind. Oceanographic observations suggest that Ekman flow in our region is generally small in comparison with geostrophic flow. Consequently, the validity of an MDT model can be tested by comparing how well it predicts current velocities compared with drifter observations. We first report quantitative tests, for which Maximenko and Niiler's oceanographic MDT model [*Maximenko and Niiler*, 2004], derived directly for drifter data, serves as a benchmark. However, the discriminating ability of the test is reduced by short-period variability: no model, not even Maximenko and Niiler's, achieves a correlation coefficient better than 50%. Table 3 summarizes the effect of suppressing the variability with a time-averaged flow from a very large number of drifter tracks over a period of many years. Alternatively, the variability can be restored

to predicted mean current flow using time variations in altimetry; the comparison is then a little less successful, with Maximenko and Niiler's correlation coefficient lowered to 44% (Table 4), probably because of the failure of altimetry to capture all shorter-period fluctuations. With both types of test, the ICM MDT model performs better than most purely oceanographic MDT models and only a little worse than Maximenko and Niiler's MDT. A test mimicking some aspects of assimilating ICM MDT into an ocean circulation model gave a mismatch with instantaneous drifter data with the same correlation coefficient as Maximenko and Niiler, 40%, and an average RMS velocity difference of 12.58 cm s^{-1} compared with Maximenko and Niiler's 12.54 cm s^{-1} (Table 4).

[55] Maps showing the predicted and observed velocity fields both display the main current streams in the Nordic seas and have a very similar structure (Figures 6a and 6b). However, the impact of smoothing on current magnitudes needs to be assessed. ICM MDT is calculated on a 2 km grid, but we smooth the output and thereby reduce the resolution in order to suppress short-wavelength noise: currents depend on a spatial derivative of MDT and derivation amplifies short wavelengths. Although we currently use a Gaussian filter with a width at half peak amplitude of 59 km (σ = 25 km), this resolution is still much better than for an MDT derived from the GRACE gravity field, which is limited to wavelengths greater than about 400 km. Smoothing smears out locally steep MDT gradients; this distributes surface boundary currents over a wider region but preserves the cumulative flow. The main region where our prediction gives significantly smaller current velocities than observed that are not attributable to smoothing a localized feature is in the flow of Atlantic waters northward toward Iceland and the Iceland-Faroe Ridge. Given the success of ICM in the Nordic seas and the rather dense gravity coverage in this part of the Atlantic, at least north of 60°N, flow in this region needs further investigation.

[56] Provided that the bathymetry is fairly uniform and the flow mainly barotropic, smoothing will not greatly distort depth-integrated transports. We require subsurface data to see whether these conditions are met and, more fundamentally, to test how well observations of depth-integrated transports compare with ICM MDT predictions.

[57] We have combined ICM MDT with historical in situ hydrographic observations from the NISE database [*Nilsen et al.*, 2008] in a novel way that estimates the absolute current velocity, volume, heat and salt transports. The classical but dubious approach assumes that there exists a surface of constant pressure at some predetermined depth. Integrating water density upward from this isobar to the geoid identifies a lateral change in surface pressure that has to be compensated for by dynamic sea surface topography. *Wunsch and Stammer* [1998] note that the flow field implied by this method fails to conserve mass and violates other physical laws. Now that we can determine MDT reliably without hydrographic input, we have a real boundary condition to replace the assumed one: we can then integrate pressure downward from the surface all the way to the bottom. Other ways of avoiding the assumption of a level of no flow through direct data inversion are being developed elsewhere [*Wunsch and Gaposchkin*, 1980; *Ganachaud et al.*, 1997; *LeGrand et al.*, 2003; *Sidorenko et al.*, 2006].

[58] We have used the NISE hydrography to calculate the 3-D baroclinic flow and then to compute transports derived in combination with ICM MDT across key cross sections in the Nordic seas. In order to reduce seasonal effects, we have restricted observations to those made over the longest time periods. We have concentrated on circulation of Atlantic water since most efforts of quantifying transports in the Nordic seas are dedicated to this water mass. With very few exceptions, our transport estimates for volume, heat and salt are close to those observed (Table 5).

[59] These tests, where our ICM MDT is imposed as a fixed boundary condition can be compared with others that properly assimilated our ICM MDT into OGCMs and then allow the system to evolve a modified MDT. The Gravity and Ocean Circulation in the Northern Atlantic project (GOCINA) included some such tests reported in [*Knudsen et al.*, 2006] where the ICM MDT was assimilated into the OGCMs DIADEM and FOAM [*Drecourt et al.*, 2006], and into the French operational forecast system MERCATOR (http://www.mercator-ocean.fr). These show that the assimilation of the ICM MDT improves the state estimation of the hydrodynamic models. The strength of testing ICM MDT by assimilation is that the OGCM checks the consistency between different components of assimilated data and the hydrodynamics used in the model. It is encouraging that the modeled MDT improves when the ICM MDT is assimilated as an indication for the quality of the ICM MDT, not just for the sections we have tested, but also for the rest of the region.

[60] Also in the near future, we anticipate a large improvement at intermediate wavelengths in geodetic MDT coming from the GOCE mission: although not reaching the wavelength resolution we get with marine gravity data, it will provide a soundly independent test for features larger than about 100 km.

[61] **Acknowledgments.** The project has been funded in part by the EU GOCINA project EVG1-CT-2002-00077 grant. The authors also wish to thank all the partners in the GOCINA project. The NISE database was provided by the Marine Research Institute, Iceland; Institute of Marine Research, Norway; the Faroese Fisheries Laboratory; and the Arctic and Antarctic Research Institute, Russia, through the NISE project.

References

Andersen, O. B., P. Knudsen, S. Kenyon, and R. Trimmer (2003), KMS2002 global marine gravity field, bathymetry and mean sea surface, paper presented at IUGG Assembly, Int. Union of Geod. and Geophys., Sapporo, Japan, 30 June to 11 July.

Baranov, V. (1957), A new method for the interpretation of aeromagnetic maps: Pseudo-gravity anomalies, *Geophysics*, *22*, 359–383.

Bingham, R. J., and K. Haines (2005), Mean dynamic topography: Intercomparisons and errors, *Philos. Trans. R. Soc.*, *364*(1841), 903–916.

Blindheim, J. (1989), Cascading of Barents Sea bottom water into the Norwegian Sea, *Rapp. Proc. Verb. Reun. Cons. Int. Explor. Mer*, *188*, 49–58.

Chelton, D. B., J. C. Ries, B. J. Haines, L.-L. Fu, and P. S. Challahan (2001), Satellite altimetry, in *Satellite Altimetry and Earth Sciences: A Handbook of Techniques and Applications*, edited by L. L. Fu and A. Cazenave, pp. 1–131, Academic, San Diego, Calif.

Drecourt, J.-P., K. Haines, and M. Martin (2006), Influence of systematic error correction on the temporal behavior of an ocean model, *J. Geophys. Res.*, *111*, C11020, doi:10.1029/2006JC003513.

Femke, C. V. (2007), Uncertainties in the mean ocean dynamic topography before the launch of the Gravity Field and Steady-State Ocean Circulation Explorer (GOCE), *J. Geophys. Res.*, *112*, C05010, doi:10.1029/2006JC003891.

Fofonoff, N. P., and R. C. Millard (1983), Algorithms for computation of fundamental properties of seawater, *UNESCO Tech. Pap. Mar. Sci.*, *44*, 1–53.

Ganachaud, A., C. Wunsch, M.-C. Kim, and B. Tapley (1997), Combination of TOPEX/POSEIDON data with a hydrographic inversion for determination of the oceanic general circulation and its relation to geoid accuracy, *Geophys. J. Int.*, *128*, 708–722.

Hansen, B., S. Østerhus, H. Hátún, R. Kristiansen, and K. M. H. Larsen (2003), The Iceland-Faroe inflow of Atlantic water to the Nordic seas, *Prog. Oceanogr.*, *59*, 443–474.

Hansen, D., and P. M. Poulain (1996), Quality control and interpolations of WOCE-TOGA drifter data, *J. Atmos. Oceanic Technol.*, *13*, 900–909.

Heiskanen, W. A., and H. Moritz (1967), *Physical Geodesy*, W. H. Freeman, San Francisco, Calif.

Hipkin, R. G., and A. Hunegnaw (2006), Mean dynamic topography by an iterative combination method, in *Proceedings of the Workshop: "GOCINA: Improving Modelling of Ocean Transport and Climate Prediction in the North Atlantic Region Using GOCE Gravimetry,"*, edited by P. Knudsen et al., *Cah. Cent. Eur. Geodyn. Seismol.*, vol. 25, pp. 135–140.

Hughes, S. L., W. R. Turrell, B. Hansen, S. Østerhus, and A. Watson (2005), Long term measurements of currents in the Faroe-Shetland Channel (1994–2002): Part 1. Initial data processing, *Fish. Res. Serv. Collab. Rep., 01/05*, Scot. Executive Fish. Res. Serv., Aberdeen, U. K.

Hunegnaw, A., and R. G. Hipkin (2006), Marine gravity network adjustment in the North Atlantic, in *Proceedings of the workshop: "GOCINA: Improving Modelling of Ocean Transport and Climate Prediction in the North Atlantic Region Using GOCE Gravimetry,"*, edited by P. Knudsen et al., *Cah. Cent. Eur. Geodyn. Seismol.*, vol. 25, pp. 11–16.

Hunegnaw, A., R. G. Hipkin, and J. Edwards (2009), A method of error adjustment for marine gravity with application to mean dynamic topography in the northern North Atlantic, *J. Geod.*, *83*, 161–174, doi:10.1007/s00190-008-0249-2.

Ingvaldsen, R. B., L. Asplin, and H. Loeng (2004a), The seasonal cycle in the Atlantic transport to the Barents Sea during the years 1997–2001, *Cont. Shelf Res.*, *24*, 1015–1032.

Ingvaldsen, R. B., L. Asplin, and H. Loeng (2004b), Velocity field of the western entrance to the Barents Sea, *J. Geophys. Res.*, *109*, C03021, doi:10.1029/2003JC001811.

Isachsen, P. E., C. Mauritzen, and H. Svendsen (2007), Dense water formation in the Nordic seas diagnosed from sea surface buoyancy fluxes, *Deep Sea Res., Part I*, *54*(1), 22–41.

Jakobsen, P. K., M. H. Ribergaard, D. Quadfasel, and T. Schmith (2003), Near-surface circulation in the northern North Atlantic as inferred from Lagrangian drifters: Variability from the mesoscale to interannual, *J. Geophys. Res.*, *108*(C8), 3251, doi:10.1029/2002JC001554.

Johannessen, J. A., et al. (2003), The European gravity field and steady state ocean circulation explorer satellite mission: Impact in geophysics, *Surv. Geophys.*, *24*, 339–386.

Jónsson, S., and H. Valdimarsson (2005), The flow of Atlantic water to the North Icelandic Shelf and its relation to the drift of cod larvae, *ICES J. Mar. Sci.*, *62*(7), 1350–1359.

Knudsen, P., et al. (2006), Geoid and ocean circulation in the North Atlantic, *Tech. Rep. 5*, Dan. Natl. Space Cent., Copenhagen.

Köhl, A., D. Stammer, and B. Cornuelle (2007), Interannual to decadal changes in the ECCO global synthesis, *J. Phys. Oceanogr.*, *37*(2), 313–337.

LeGrand, P., E. J. O. Schrama, and J. Tournadre (2003), An inverse estimate of the dynamic topography of the ocean, *Geophys. Res. Lett.*, *30*(2), 1062 doi:10.1029/2002GL014917.

Maximenko, N., and P. P. Niiler (2004), Hybrid decade-mean global sea level with mesoscale resolution, in *Recent Advances in Marine Science and Technology*, edited by N. Saxena, pp. 55–59, PACON Int., Honolulu, Hawaii.

Mork, K. A., and J. Blindheim (2000), Variations in the Atlantic inflow to the Nordic seas, 1955–1996, *Deep Sea Res., Part I*, *47*(6), 1035–1057, doi:10.1016/S0967-0637(99)00091-6.

Niiler, P. P., and J. D. Paduan (1995), Wind-driven motions in the northeast Pacific as measured by Lagrangian drifters, *J. Phys. Oceanogr.*, *25*, 2819–2830.

Niiler, P. P., A. Sybrandy, K. Bi, P. Poulain, and D. Bitterman (1995), Measurements of the water-following capability of holey-sock and TRISTAR drifters, *Deep Sea Res.*, *42*, 1951–1964.

Nilsen, J. E. Ø., H. Hàtùn, K. A. Mork, and H. Valdimarsson (2008), The NISE Dataset, *Tech. Rep., 08-01*, 17 pp., Faroese Fish. Lab., Törshavn, Faroe Islands.

Nøst, O. A., and P. E. Isachsen (2003), The large-scale time-mean ocean circulation in the Nordic seas and Arctic Ocean estimated from simple dynamics, *J. Mar. Res.*, *61*, 175–210.

O'Dwyer, J., Y. Kasajima, and O. A. Nøst (2001), North Atlantic Water in the Barents Sea opening, 1997 to 1999, *Polar Res.*, *20*(2), 209–216.

Orvik, K. A., and Ø. Skagseth (2003), The impact of the wind stress curl in the North Atlantic on the Atlantic inflow to the Norwegian Sea toward the Arctic, *Geophys. Res. Lett.*, *30*(17), 1884, doi:10.1029/2003GL017932.

Orvik, K. A., and Ø. Skagseth (2005), Heat flux variations in the eastern Norwegian Atlantic Current toward the Arctic from moored instruments, 1995–2005, *Geophys. Res. Lett.*, *32*, L14610, doi:10.1029/2005GL023487.

Orvik, K. A., Y. Skagseth, and M. Mork (2001), Atlantic inflow to the Nordic seas: Current structure and volume fluxes from moored current meters, VM-ADCP and SeaSoar-CTD observations, 1995–1999, *Deep Sea Res., Part I*, *48*(4), 937–957.

Østerhus, S., W. R. Turrell, S. Jónsson, and B. Hansen (2005), Measured volume, heat, and salt fluxes from the Atlantic to the Arctic Mediterranean, *Geophys. Res. Lett.*, *32*, L07603, doi:10.1029/2004GL022188.

Otto, L., and H. M. van Aken (1996), Surface circulation in the northeast Atlantic Ocean as observed with drifters, *Deep Sea Res., Part I*, *43*, 467–499.

Rio, M. H., and F. Hernandez (2004), A mean dynamic topography computed over the world ocean from altimetry, in situ measurements, and a geoid model, *J. Geophys. Res.*, *109*, C12032, doi:10.1029/2003JC002226.

Saunders, P. M. (1990), Cold outflow from the Faroe Bank channel, *J. Phys. Oceanogr.*, *20*, 29–43.

Saunders, P. M., A. C. Coward, and B. A. de Cuevas (1999), Circulation of the Pacific Ocean seen in a global model: Ocean Circulation and Climate Advanced Modelling Project (OCCAM), *J. Geophys. Res.*, *104*(C8), 18,281–18,299.

Sidorenko, D., S. Danilov, G. Kivman, and J. Schröter (2006), On the use of a deep pressure gradient constraint for estimating the steady state ocean circulation from hydrographic data, *Geophys. Res. Lett.*, *33*, L02610, doi:10.1029/2005GL024716.

Skagseth, Ø., T. Furevik, R. Ingvaldsen, H. Loeng, K. A. Mork, K. A. Orvik, and V. Ozhigin (2008), Volume and heat transports to the Arctic Ocean via the Norwegian and Barents Seas, in *Arctic-Subarctic Ocean Fluxes: Defining the Role of the Northern Seas in Climate*, edited by R. Dickson, J. Meincke, and P. Rhines, pp. 45–64, Springer, Dordrecht, Netherlands.

Sybrandy, A. L., and P. P. Niiler (1990), The WOCE/TOGA Lagrangian drifter construction manual, *WOCE Rep., 63*, 58 pp., Scripps Inst. of Oceanogr., Univ. of Calif., San Diego, La Jolla, Calif.

Tapley, B., and M. C. Kim (2001), Applications to geodesy, in *Satellite Altimetry and Earth Sciences*, edited by L. L. Fu and A. Cazenave, pp. 371–403, Academic, San Diego, Calif.

Tapley, B. D., S. Bettadpur, J. C. Ries, P. F. Thompson, and M. M. Watkins (2004), GRACE measurements of mass variability in the Earth system, *Science*, *305*, 503–505.

Turrell, W. R., B. Hansen, S. Hughes, and S. Østerhus (2003), Hydrographic variability during the decade of the 1990's in the northeast Atlantic and southern Norwegian Sea, *ICES Mar. Sci. Symp.*, *219*, 111–120.

Wunsch, C. (2006), *Discrete Inverse and State Estimation Problems: With Geophysical Fluid Applications*, 384 pp., Cambridge Univ. Press, Cambridge, U. K.

Wunsch, C., and E. M. Gaposchkin (1980), On using satellite altimetry to determine the general cimulation of the oceans with applications to geoid improvements, *Rev. Geophys.*, *18*, 725–745.

Wunsch, C., and D. Stammer (1998), Satellite altimetery, the marine geoid and the oceanic general circulation, *Annu. Rev. Earth Planet. Sci.*, *26*, 219–254.

R. Hipkin and A. Hunegnaw, School of GeoSciences, University of Edinburgh, West Mains Road, Edinburgh EH9 3JW, UK. (addisu.hunegnaw@ed.ac.uk)

K. A. Mork, Bjerknes Centre for Climate Research, Allégaten 55, N-5007 Bergen, Norway.

F. Siegismund, Center for Marine and Atmospheric Science, Institute of Oceanography, University of Hamburg, Bundesstrasse 53, D-20146 Hamburg, Germany.